Copy
RM L53B17

RESEARCH MEMORANDUM

THE EFFECT OF BLADE-SECTION CAMBER ON THE STALL-FLUTTER CHARACTERISTICS OF THREE NACA PROPELLERS AT ZERO ADVANCE

By Arthur E. Allis and John M. Swihart

Langley Aeronautical Laboratory
Langley Field, Va.

NATIONAL ADVISORY COMMITTEE
FOR AERONAUTICS

WASHINGTON

April 6, 1953

NATIONAL ADVISORY COMMITTEE FOR AERONAUTICS

RESEARCH MEMORANDUM

THE EFFECT OF BLADE-SECTION CAMBER ON THE STALL-FLUTTER CHARACTERISTICS OF THREE NACA PROPELLERS AT ZERO ADVANCE

By Arthur E. Allis and John M. Swihart

SUMMARY

An investigation to determine the effect of blade-section camber on the stall-flutter characteristics of three propellers has been conducted on the 6,000-horsepower propeller dynamometer at the Langley propeller static test stand at zero advance. These propellers were the NACA 10-(0)(066)-03, 10-(3)(066)-03, and 10-(5)(066)-03, all 10 feet in diameter, having two blades, constant chord, and a constant design lift coefficient from root to tip of 0, 0.3, and 0.5, respectively. The blade-angle range was from 16° to 38° measured at the 0.75 radius. The propeller rotational speed was increased in even increments until flutter occurred.

The results indicated that an increase in blade-section camber produced an increase in flutter-speed coefficient for blade-angle settings up to 28°. There was a 36-percent increase in thrust coefficient at flutter with an increase in blade-section design lift coefficient from 0 to 0.5 at a blade angle of 16°.

The NACA 10-(0)(066)-03 propeller was operated in the flutter region and there was an increase in thrust with an increase in tip Mach number. The propeller tip Mach number was increased by increasing the propeller rotational speed. A rapid rise in torsional stress with an increase in tip Mach number while operating in the flutter region was noted.

INTRODUCTION

In the design of a supersonic-type propeller primary consideration has been given to reducing blade-section thickness ratios to as low a value as stress considerations would permit. However, the propeller with very thin sections has a low value of torsional rigidity and is susceptible

to stall flutter; consequently the attainment of satisfactory take-off characteristics may be a difficult problem. In an effort to improve the flutter characteristics of propellers and yet maintain thin blade sections, parameters other than design lift coefficient have been varied and their effect studied (ref. 1). Recent propeller tests at the Langley propeller static test stand (ref. 2) indicated that an increase in blade-section camber had a beneficial effect on propeller stall-flutter characteristics at the one blade angle (16°) at which flutter was encountered.

The purpose of the present investigation was to extend the work of reference 2 on propeller flutter characteristics to higher blade angles. The tests were conducted at the Langley propeller static test stand on the 6,000-horsepower dynamometer. Three propellers, all 10 feet in diameter and similar in every respect except blade-section camber (or design lift coefficient), were investigated. During the tests simultaneous measurements of thrust, torque, blade torsional deflection, torsional stress, and bending stress were made at successive values of rotational speed below that at which stall flutter occurred, at stall flutter, and for a few tests beyond the occurrence of stall flutter. The tests covered a blade-angle range from 16° to 38° at tip Mach numbers up to 0.72. Propeller tip Mach number was varied by varying the propeller rotational speed.

SYMBOLS

a	speed of sound, ft/sec
b	blade width (chord), ft
b_r	blade-section semichord at the 0.837 radial station, ft
c	length of line normal to both the propeller blade axis and a plane containing the light source (see fig. 13)
C_P	power coefficient, $P/\rho n^3 D^5$
C_T	thrust coefficient, $T/\rho n^2 D^4$
C_T/C_P	static-thrust figure of merit
c_{l_d}	section design lift coefficient
D	propeller diameter, ft

[redacted]

h	blade-section maximum thickness, ft
M_t	tip Mach number (based on rotational speed of propeller tip), $\pi nD/a$
n	propeller rotational speed, rps
N	propeller rotational speed, rpm
P	power, ft-lb/sec
r	radius to a blade element, ft
R	propeller-tip radius, ft
t	time difference between signal from reference prism and signal from prism at 0.70 radius
T	thrust, lb
V	blade-section velocity at 0.837 radius
x	fraction of tip radius, r/R
y	distance from propeller rotational axis to horizontal plane through light source (see fig. 13)
z	horizontal distance from light source to plane of rotation of propeller (see fig. 13)
β_x	blade angle at station x, deg
$\Delta\beta$	torsional deflection, deg
ϵ	angle in propeller plane between blade in lower vertical position and any other angular position, deg
ρ	air density, slugs/cu ft
θ	$\tan^{-1} c/z$, deg
ω_α	blade natural torsional frequency, radians/sec

Subscripts:

0	reference or zero operating condition
1	any operating condition other than reference condition

[redacted]

APPARATUS AND METHODS

Three 2-blade duralumin 10-foot-diameter propellers were tested on one unit of the Langley 6,000-horsepower propeller dynamometer. A detailed description of this dynamometer is given in reference 2. Figure 1 shows one of the propellers used in the present investigation installed on the dynamometer.

Propeller blades.- Three propellers differing only in blade-section camber, the NACA 10-(0)(066)-03, 10-(3)(066)-03, and 10-(5)(066)-03, were used for the present tests and were identical to those used in reference 2. The numerical designation is an indication of the propeller geometry and the airfoil section at the design radius ($r/R = 0.70$). The propellers are all 10 feet in diameter, have constant radial design lift coefficients of 0, 0.3, and 0.5, and incorporate NACA 16-series airfoil sections. The blade sections at the 0.7 radius are 6.6 percent thick and have a solidity of 0.03 per blade. One blade of each propeller contained pressure tubes (as described in ref. 3) and is referred to as the tubed blade in this paper. The other blade, which was solid, is referred to as the untubed blade. The blade-form curves for these propellers are given in figure 2.

Strain-gage instrumentation.- The NACA 10-(0)(066)-03 propeller had one bending and one torsion gage on each blade; whereas the 0.3 and 0.5 cambered propellers had one bending and one torsion gage on only the untubed blade. The bending gage was attached to the thrust face of the blade at the 0.30 radius and measured combined stress (steady plus vibratory). The torsion gage was fixed to the cambered face of the blade also at the 0.30 radius and measured steady plus vibratory torsional stress. The bending-stress limit was set at 15,000 psi, and the torsional-stress limit was set at 5,000 psi, steady plus vibratory. A typical record of torsional stress obtained during a test is shown in figure 3.

Torsional deflection.- The torsional deflections of the propeller blades at the 0.7 radius were measured by an optical deflectometer. A complete description and operating procedure for the optical deflectometer is given in the appendix.

Test conditions.- The blade-angle range covered was from 16° to 38° in increments of 2° or 4° measured at the 0.75 radius. The rotational speed was varied in even intervals until flutter occurred at each blade angle. Flutter was detected by audible means and by visual observation of the strain-gage recorder. Thrust, torque, blade-torsional deflection, and bending and torsional stress were measured at each rotational speed up to and including the flutter point for each blade angle. Stress readings were taken on the NACA 10-(0)(066)-03 propeller while taking points every 50 rpm higher than the flutter point until the torsional-stress

limit was reached. Tests were not conducted in inclement or gusty weather or when the steady wind velocity exceeded 5 mph.

Accuracy of measurements.- In general, the speed at which flutter occurred, for a given blade-angle setting, could be repeated with an accuracy of 5 percent. A few repeat points differed by as much as 10 percent.

The values of thrust coefficient and power coefficient at which flutter was first detected could be repeated with an accuracy of 5 percent.

The propeller blade angle was set with an accuracy of $\pm 0.05^\circ$, and propeller blade torsional deflection was measured with an accuracy of about $\pm 0.10^\circ$.

RESULTS AND DISCUSSION

In presenting the results of the flutter investigation the ratio $V/b_r\omega_\alpha$, designated as the flutter-speed coefficient in reference 1, is herein employed. The value of V is the blade-section velocity at the 0.837 radial station and is calculated for the rotational speed at which flutter was first encountered. The 0.837 radial station was chosen to place the results of this investigation on the same coefficient basis as the results of reference 1. In reference 1 the velocity was measured at a reference station which was 0.80 of the effective length of the blade from the spinner surface. In this paper the 0.837 radial station is equal to 0.80 of the effective blade length where, in the absence of a spinner, the effective length is taken as the distance from the first inboard airfoil section to the blade tip.

Where the data in this report are presented as a function of tip Mach number, a secondary scale is also given for approximate values of propeller rotational speed corresponding to the tip Mach number values. Since Mach number is such an important parameter in flutter work, it should be emphasized that tip Mach number was varied by varying propeller rotational speed and does not solely indicate a Mach number effect, but rather all the effects of increased rotational speed.

A static-bench test revealed that the values of ω_α for the three propellers tested were about the same. A maximum variation between the three blade designs of 2 percent in ω_α was found. The measured values of ω_α for each propeller blade are given in the following table:

Propeller	ω_α for tubed blade, radians/sec	ω_α for untubed blade, radians/sec
NACA 10-(0)(066)-03	942.5	978.9
NACA 10-(3)(066)-03	956.0	981.0
NACA 10-(5)(066)-03	936.2	961.3

It is believed that this variation is probably due to slight differences in fabrication between the propeller blades since there was no systematic variation of ω_α with blade camber. A value of ω_α calculated by the method of reference 4 was found to be 6 percent higher than the measured value. The measured values of ω_α have been used for all data reduction in this paper since the measurements could be repeated to ± 1 cps. The data presented are based on ω_α for the tubed blade since it had a lower value of ω_α than the untubed blade and, therefore, would be more susceptible to flutter.

In reference 1 the characteristics of stall flutter and classical flutter are given. Stall flutter is characterized by high angle-of-attack operation and a flutter frequency nearly the same as the natural first-torsion frequency of the blade. The flutter data presented in this report have been termed stall flutter because of the high section angles of attack at which flutter was obtained, and also because the measured torsional frequency at flutter agreed within the accuracy of the measurements with the natural first-torsion frequency of the blade.

The effect of camber on the propeller flutter characteristics.- The variation of flutter-speed coefficient with blade angle for the three propellers tested is shown in figure 4. There is a 45-percent increase in flutter-speed coefficient at a blade angle of 16° for the 0.5 cambered blade when compared with the symmetrical blade. The difference between the flutter-speed coefficient of the cambered blade and the symmetrical blade decreases with increasing blade angle. At $\beta_{0.75R} = 30°$ the coefficients are almost the same $\left(V/b_r\omega_\alpha \approx 1.00\right)$. At $\beta_{0.75R} = 30°$ and above, all sections of the blade are stalled for zero-advance operation but at $\beta_{0.75R} = 16°$ only the inboard sections of the blade are stalled. Beyond 30° there is an increase in flutter-speed coefficient for the three propellers. The minimum value of flutter-speed coefficient obtained during the tests was very nearly 1.00, which agreed with the experimental results of reference 1. Tip Mach numbers corresponding to the flutter-speed coefficient as shown in figure 4 are presented in figure 5.

[redacted]

An increase in flutter-speed coefficient for the propellers tested at a given blade angle is not important in itself unless accompanied by an increase in propeller thrust. The variation of thrust coefficient with tip Mach number up to the flutter point for the three propellers tested at $\beta_{0.75R} = 16^\circ$ is shown in figure 6. Because the propeller delivering the highest thrust induces a higher velocity through the propeller for a given rotational tip speed, the effective angle of attack of the blade is reduced and allows the blade sections to operate at higher rotational speeds before flutter occurs. The thrust data obtained at the onset of flutter, as shown in figure 7, up to $\beta_{0.75R} = 24^\circ$ indicated an increase in thrust and thrust coefficient at flutter with an increase in blade camber at the same blade-angle setting for the three propellers. At $\beta_{0.75R} = 16^\circ$ an increase of 36 percent in thrust coefficient and a 45-percent increase in tip Mach number in going from the symmetrical propeller to the propeller with a design lift coefficient of 0.5 was realized. This increase in thrust coefficient and tip Mach number increases the thrust from 640 pounds for the symmetrical propeller to 1,835 pounds for the propeller having a design lift coefficient of 0.5. This is a 187-percent increase in thrust at flutter. A part of the increase in thrust is due to the higher rotational speed attained by the cambered propeller before flutter occurred and the remaining increase can be attributed to the increase in thrust coefficient. At $\beta_{0.75R} = 28^\circ$ and above, the values of thrust coefficient were about equal. The data for blade angles above 24° have not been presented in graphical form because they are felt to be of minor importance for practical operating conditions; however, table I presents the values of C_T, C_P, and M_t obtained at flutter for each blade angle during the present investigation.

The static-thrust figure of merit C_T/C_P is an indication of propeller effectiveness at zero advance; however, it is of secondary importance except when comparing flutter-free propellers or propellers that encounter flutter at the same power coefficient. When flutter is a limiting factor in propeller operation, that is, if the full power available cannot be absorbed, the propeller that produces the most thrust is to be favored for the zero-advance condition. If the propeller that produces the most thrust does so with relatively less power than the other propellers under consideration, there is no question of its superiority at the zero-advance condition of operation. In figure 8, values of C_T/C_P obtained at the first indication of flutter for the three propellers are shown for blade angles of 16°, 20°, and 24°. This figure shows that increasing blade camber also increases the ability of a propeller to produce thrust effectively. This is the result of more favorable lift-drag ratios of the cambered sections at subsonic Mach numbers.

[redacted]

Effect of operation in the flutter region on thrust and power coefficients.- One propeller, the NACA 10-(0)(066)-03, was operated in the flutter region. The effect of an increase in tip Mach number before and after the first indication of flutter on the thrust coefficient, power coefficient, and C_T/C_P at $\beta_{0.75R} = 16^\circ$, 20°, and 24° is shown in figure 9. It appears that beyond the first flutter point and into the flutter region the slope of the lift curve remains positive to a higher angle of attack for an oscillating airfoil since there is a definite increase in thrust coefficient. This conclusion is confirmed by the results of reference 5 for an airfoil oscillated in pure pitch. Increasing the tip Mach number in the flutter region produced an increase in power coefficient for $\beta_{0.75R} = 20^\circ$ and 24°. At $\beta_{0.75R} = 16^\circ$ there was no apparent increase in power coefficient with tip Mach number up to $M_t = 0.575$. The ratio C_T/C_P increases slightly with rotational speed for the three blade angles until the first indication of flutter. Raising the speed above the first flutter point decreased the value of C_T/C_P for the blade angles of 20° and 24°, but at the blade angle of 16° there is a slight increase in C_T/C_P.

Effect of operation in the flutter region on torsional stress.- The effect of increasing the rotational speed on the torsional shear stress for the NACA 10-(0)(066)-03 propeller at blade angles of 16° and 20° is shown in figure 10. It can be seen that the stress remains at a relatively low value until flutter occurs, but with a further increase in tip Mach number the stress rises rapidly. Increasing the propeller tip Mach number from 0.425 (first flutter point) to 0.516 produced an increase in torsional stress from 640 psi to 3,580 psi for the untubed blade at $\beta_{0.75R} = 20^\circ$. Further increases in tip Mach number would certainly have led to destruction of the equipment. In general, the three propellers entered the flutter region smoothly and a definite sine-wave pattern of torsional stress could be seen on the strain-gage recorder (see fig. 3). As the rotational speed was increased, the magnitude of the peak-to-peak stresses increased, as did the noise level at the test facility; however, unpublished data taken on another thinner propeller (NACA 10-(3)(049)-03) showed no gradual entry into the flutter region with increases in rotational speed. This thinner propeller encountered violent flutter at blade angles as low as 12° and the accompanying shear-stress pattern was very large. The beating noise accompanying flutter was loud and easily distinguished from ordinary propeller noise.

Blade torsional deflection.- Blade torsional deflections were measured at the 0.7 radius during the operation of the three test propellers. There was no appreciable torsional deflection in any of the blades when the static blade angle was set at 20° or higher (fig. 11). At the blade angle of 16° about $1/2^\circ$ of blade twist was measured on the NACA 10-(5)(066)-03 propeller. A calculated value of blade torsional deflection,

in which only centrifugal effects were considered, showed that at the low rotational speed taken as a reference zero the deflection would be less than 0.05° at the 0.70 radius. Blade steady torsional deflection does not appear to have any influence on the flutter characteristics of these test propellers at the higher blade angles. However, unpublished tests of a thinner propeller (NACA 10-(3)(049)-03) show that there is a blade torsional deflection of a magnitude that would increase the blade angle and could cause a blade to flutter at lower rotational speeds.

CONCLUSIONS

An investigation to determine the effect of blade-section design lift coefficient on the stall-flutter characteristics of three NACA propellers at zero advance has led to the following conclusions:

1. For blade-angle settings from 16° to 28° there was an increase in flutter-speed coefficient with an increase in blade-section design lift coefficient.

2. An increase in blade-section design lift coefficient gave an increase both in thrust coefficient and in absolute thrust at the onset of flutter for blade angles from 16° to 24°. At a blade angle of 16°, measured at the 0.75 radial station, there was a 36-percent increase in thrust coefficient and a 187-percent increase in thrust at flutter when the blade-section design lift coefficient was increased from 0 to 0.5.

3. The use of camber in the blade design increases the static-thrust figure of merit at the onset of flutter.

4. Operation in the flutter region gave an increase in thrust coefficient with an increase in tip Mach number.

5. Torsional-stress measurements showed a rapid rise in magnitude with increasing tip Mach number beyond the speed at which flutter was first detected.

Langley Aeronautical Laboratory,
National Advisory Committee for Aeronautics,
Langley Field, Va.

[redacted]

APPENDIX

DESCRIPTION AND OPERATING PROCEDURE OF OPTICAL DEFLECTOMETER

General description.- The method used to measure the torsional deflection of the propeller blades tested involves the use of a concentrated arc light source, a photoelectric cell, an electronic counter, and focusing prisms mounted on the propeller hub and blade. The light source and photoelectric cell were enclosed inside a protective fairing which was mounted at the leading edge of the dynamometer support strut. Reference to figure 12 gives the location of some of the components of the optical deflectometer inside the fairing. Light from a 100-watt concentrated arc light source is focused by an f:1 lens on a small prism mounted on the photoelectric cell. The light leaves the prism and forms a large cone of light at the propeller blade. When the light rays in the cone are normal to the prisms on the hub and propeller blade, light is reflected back to the photoelectric cell where the light signals are converted to electrical signals. The signals are then fed into an electronic counter (not shown in fig. 12) which measured the time difference in microseconds between the signal from the blade prism and the reference prism mounted on the hub. The optical deflectometer as used during the present investigation did not measure absolute blade angle but did measure the change in blade angle from a reference condition of operation to any operating condition. Generally the reference condition of operation was chosen at the lowest propeller rotational speed that could be accurately determined.

Light source.- It was necessary to use a 100-watt concentrated arc light source during the present tests in order to obtain a large cone of high-intensity light at the propeller disk and also to obtain a very small returning spot of light at the photoelectric cell from the hub and propeller-blade prisms.

Photoelectric cell.- The multiplier photoelectric cell was carefully adjusted so that the light signals from the prisms would strike the sensitive area of the cell.

Electronic counter.- Accurate measurements of the time interval between two electrical signals were obtained by using an electronic counter. The electronic counter could accurately measure time differences between signals to 0.6 microsecond. Instantaneous readings were obtained during the tests and the readings were recorded visually.

[redacted]

Prisms.- The right-angle prisms used were a special type having a lens surface bonded to the hypotenuse face with a focal length equal to the distance from the prism to the photoelectric cell. Through use of a lens surface on the prisms a small returning spot of light registered on the photoelectric cell. The reference prism was mounted on the propeller hub and had a length of 1/2 inch and hypotenuse face 1/4 inch wide. The reference prism was mounted so that the long axis was perpendicular to the radial axis of the propeller blade and the hypotenuse face exposed to the light rays. When the reference prism was properly mounted the light signal registered on the photoelectric cell when the propeller blade was in the bottom vertical position.

The propeller-blade prism was mounted at the 0.70 radial station on the propeller blade that was retained in the hub barrel containing the reference prism. The smallest possible prism was used on the propeller blade to minimize the influence of the prism on the air flow. The propeller-blade prism was 1/2 inch long and the width of the hypotenuse face was 1/8 inch. The blade prism was mounted with its long axis perpendicular to the propeller blade radial axis as was the reference prism.

Geometry.- A schematic diagram showing the location of the protective fairing at the base of the dynamometer and the geometry of the setup is shown in figure 13. Referring to figure 13, the length of line y is the perpendicular distance from the axis of rotation to the photoelectric cell. The length of line z is the horizontal distance from the plane of rotation to the photoelectric cell. The angle ϵ is determined by the time interval between the reference signal and the signal from the prism at the 0.70 radial station for a given rotational speed. The reference signal registered on the photoelectric cell when the blade was in the bottom vertical position; whereas the signal from the propeller blade registered when it was in a position counterclockwise from bottom center (looking at the propeller disk from the rear). The greater the blade-angle setting at the $x = 0.70$ radius the larger the value of ϵ. If $\beta_{0.70R} = 0^{\circ}$ and the prism at the 0.70 radial station was mounted so that its long axis was exactly parallel to the blade chord, then the reference signal and the signal from the prism at the 0.70 radial station would be coincident at the photoelectric cell. When $\beta_{0.70R}$ is set at some positive value, the signal from the blade prism would register on the photoelectric cell and then as the blade continues to the bottom vertical position the signal from the reference prism registers on the photoelectric cell. The angle ϵ can be calculated from $\epsilon = 360\ nt$ if the time difference between signals and the propeller rotational speed are known.

After the angle ϵ and the length of line y have been determined, the length of line c shown in figure 13 can be calculated since line c

[redacted]

is normal to the propeller blade axis and also lies in the plane of rotation. When the length of line c has been determined, the angle θ may be calculated ($\theta = \tan^{-1} c/z$). The value of θ will vary directly as the blade angle at the 0.70 radial station. During the present tests blade torsional deflection $\Delta\beta$ was determined as the difference between θ at any operating condition θ_1 and θ at the reference condition of operation θ_0. Therefore,

$$\Delta\beta = \theta_1 - \theta_0 = \tan^{-1} \frac{y}{z}\left[\sin\left(360n_1t_1\right) - \sin\left(360n_0t_0\right)\right]$$

The major error that would occur in measuring $\Delta\beta$ due to blade bending is eliminated through use of a prism on the propeller blade since the light paths to and from the prism will be parallel when high-quality right-angle prisms are used.

It must be pointed out that the point E (fig. 13) is not necessarily at the prism location. The location of E is determined by the intersection of the perpendicular from F to the blade axis at the instant the prism axis is normal to the plane LED. This is the instant at which the signal is returned to the photoelectric cell. It should be kept in mind that a signal will always be returned to the photoelectric cell regardless of the radial location of the prism on the blade because of the property of the prism of returning the light in the plane containing the axis of the prism and the source of light.

Operating procedure.- The measurements of blade torsional deflection could not be made during the daylight hours because the light signals, even on cloudy days, were too weak to register on the photoelectric cell. During the tests, readings were taken on the electronic counter only when the propeller rotational speed was fixed at the speed desired. Five readings were taken on the electronic counter and the results averaged to give the average time interval for the test condition. When the optical deflectometer was first used, considerable difficulty was encountered due to vibration of the various components inside the protective fairing. This problem was solved through adequate shock mounting of the components.

REFERENCES

1. Baker, John E.: The Effects of Various Parameters Including Mach Number on Propeller-Blade Flutter With Emphasis on Stall Flutter. NACA RM L50L12b, 1951.

2. Wood, John H., and Swihart, John M.: The Effect of Blade-Section Camber on the Static Characteristics of Three NACA Propellers. NACA RM L51L28, 1952.

3. Maynard, Julian D., and Murphy, Maurice P.: Pressure Distributions on the Blade Sections of the NACA 10-(3)(066)-033 Propeller Under Operating Conditions. NACA RM L9L12, 1950.

4. Houbolt, John C., and Anderson, Roger A.: Calculation of Uncoupled Modes and Frequencies in Bending or Torsion of Nonuniform Beams NACA TN 1522, 1948.

5. Halfman, Robert L., Johnson, H. C., and Haley, S. M.: Evaluation of High-Angle-of-Attack Aerodynamic-Derivative Data and Stall-Flutter Prediction Techniques. NACA TN 2533, 1951.

[redacted]

TABLE I

MEASURED VALUES OF M_t, C_T, AND C_P AT THE FIRST INDICATION OF FLUTTER

NACA 10-(0)(066)-03				NACA 10-(3)(066)-03				NACA 10-(5)(066)-03			
$\beta_{0.75R}$, deg	M_t	C_T	C_P	$\beta_{0.75R}$, deg	M_t	C_T	C_P	$\beta_{0.75R}$, deg	M_t	C_T	C_P
16	0.485	0.078	0.056	16	0.608	0.096	0.058	16	0.701	0.109	0.064
16	.485	.081	.055	16	.613	.098	.059	16	.711	.105	.062
20	.424	.094	.085	20	.460	.106	.081	20	.476	.117	.088
20	.410	.096	.085	20	.455	.107	.084	20	.493	.111	.084
24	.349	.111	.120	24	.387	.119	.117	24	.392	.124	.107
24	.355	.111	.119	24	.382	.120	.118	24	.403	.123	.109
28	.346	.119	.152	28	.358	.123	.145	28	.367	.116	.136
28	.334	.116	.147	30	.359	.126	.158	30	.356	.118	.153
30	.338	.128	.180	32	.344	.125	.174	32	.358	.124	.173
30	.338	.119	.186	34	.356	.123	.185	34	.350	.131	.193
32	.342	.125	.187	38	.368	.124	.218	38	.385	.132	.227
34	.364	.126	.207								
34	.367	.119	.195								
38	.435	.127	.237								
38	.432	.125	.230								

Figure 1.- Propeller mounted on one unit of the Langley 6,000-horsepower propeller dynamometer.

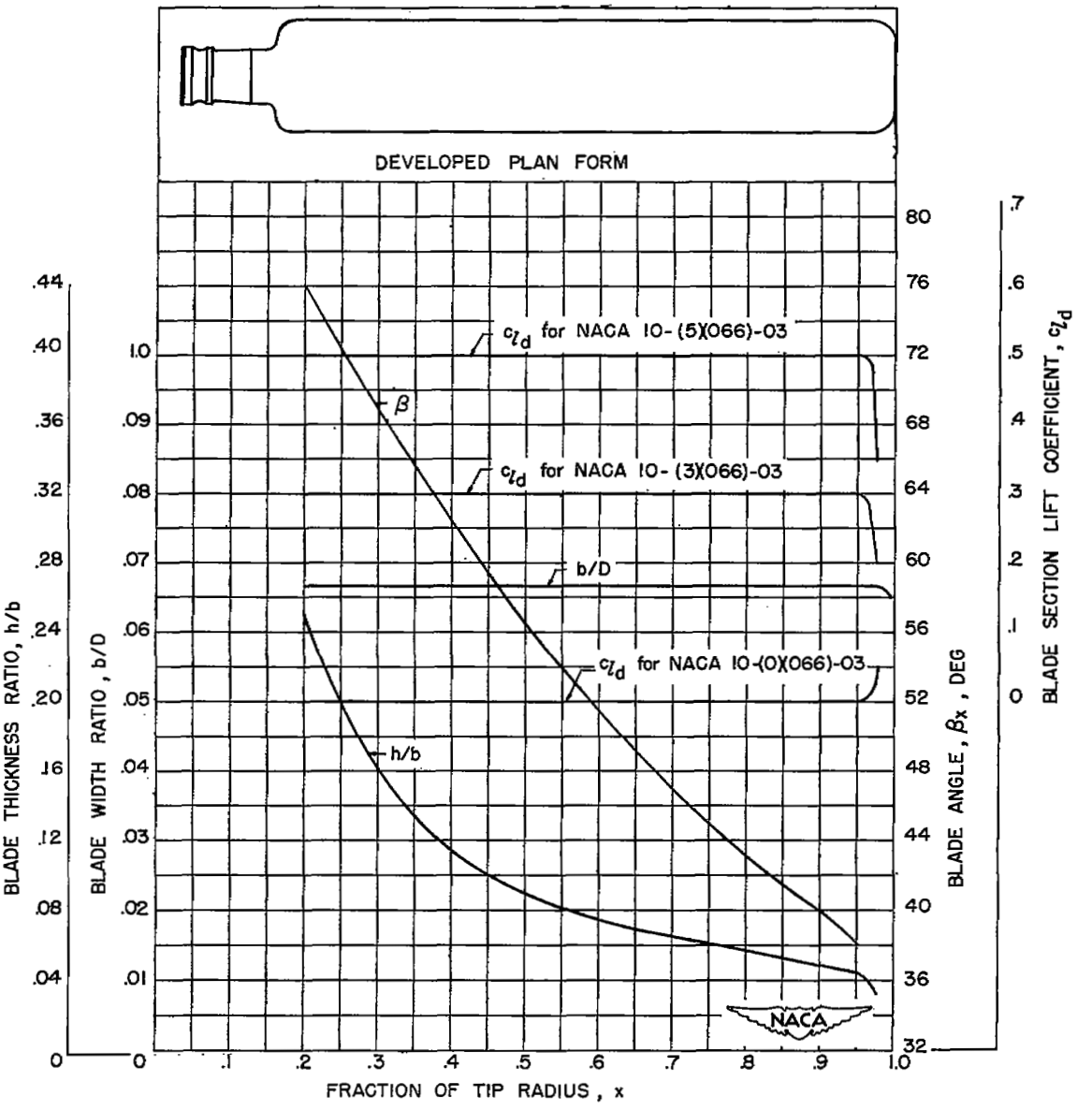

Figure 2.- Blade-form curves for NACA 10-(5)(066)-03, NACA 10-(3)(066)-03, and NACA 10-(0)(066)-03 propellers.

[redacted]

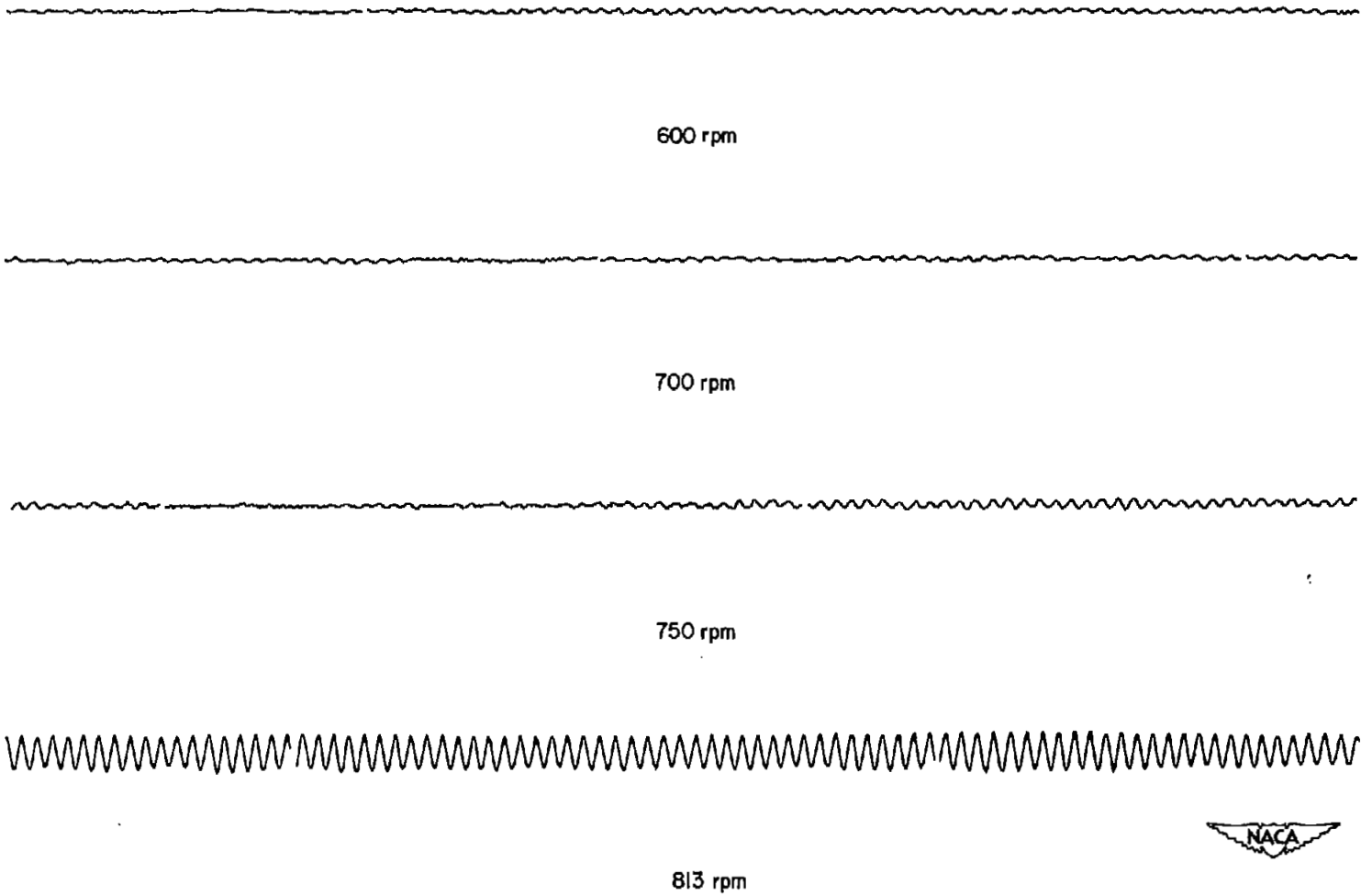

Figure 3.- A typical torsional-stress record showing flutter at 813 rpm.

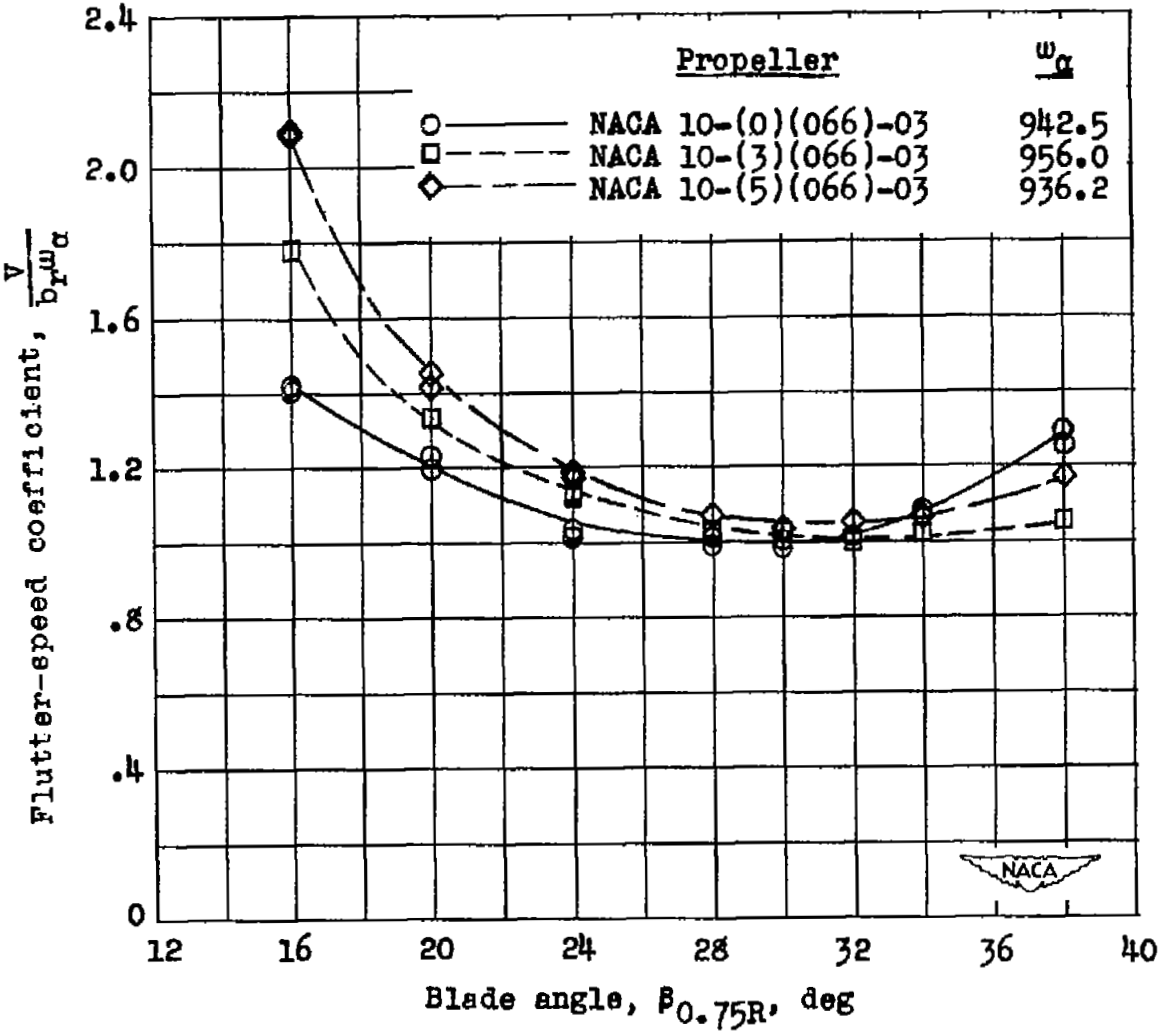

Figure 4.- Variation of flutter-speed coefficient with blade angle for the three test propellers.

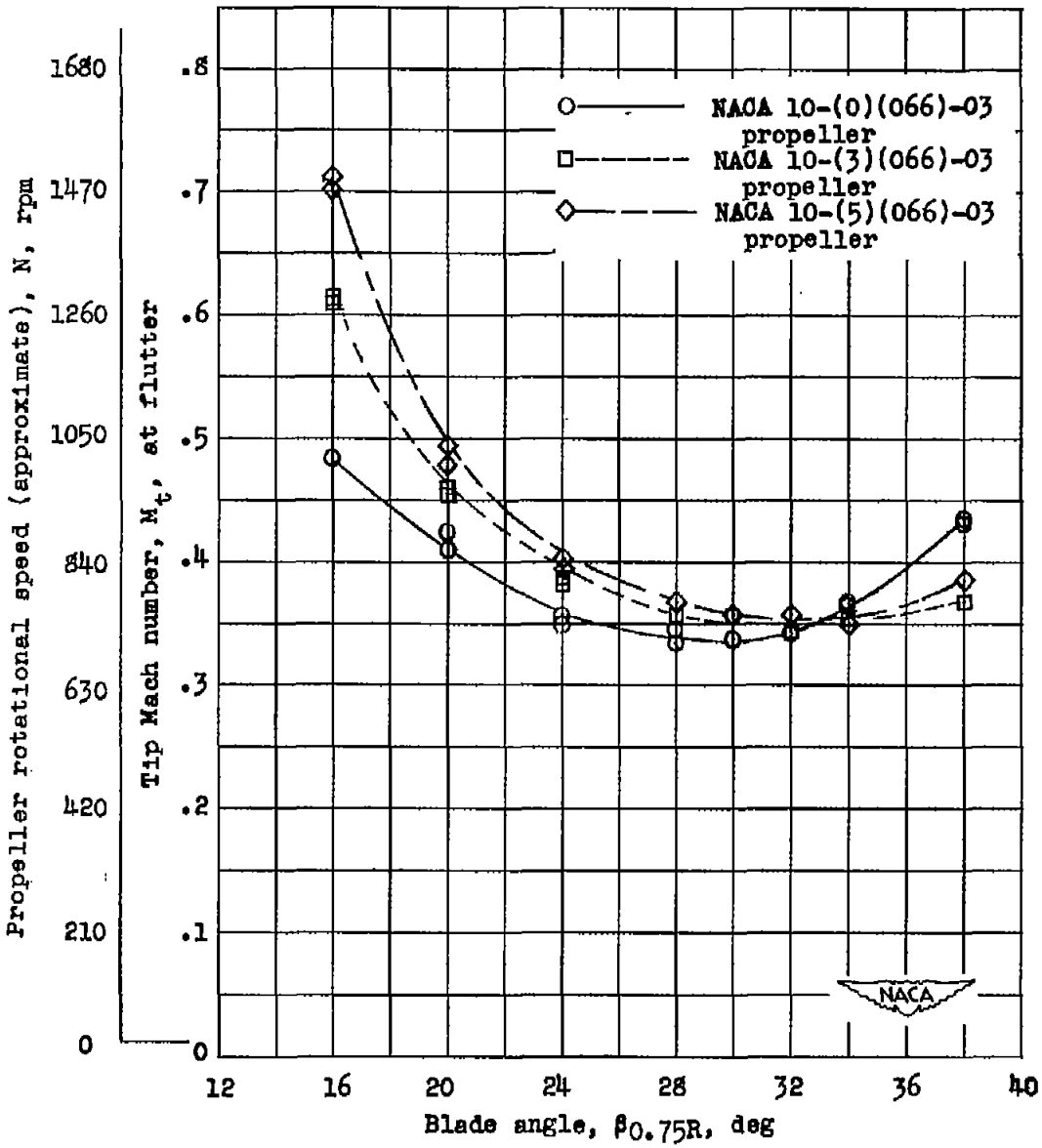

Figure 5.- Variation of tip Mach number (or approximate propeller rotational speed) at flutter with blade angle of the three test propellers.

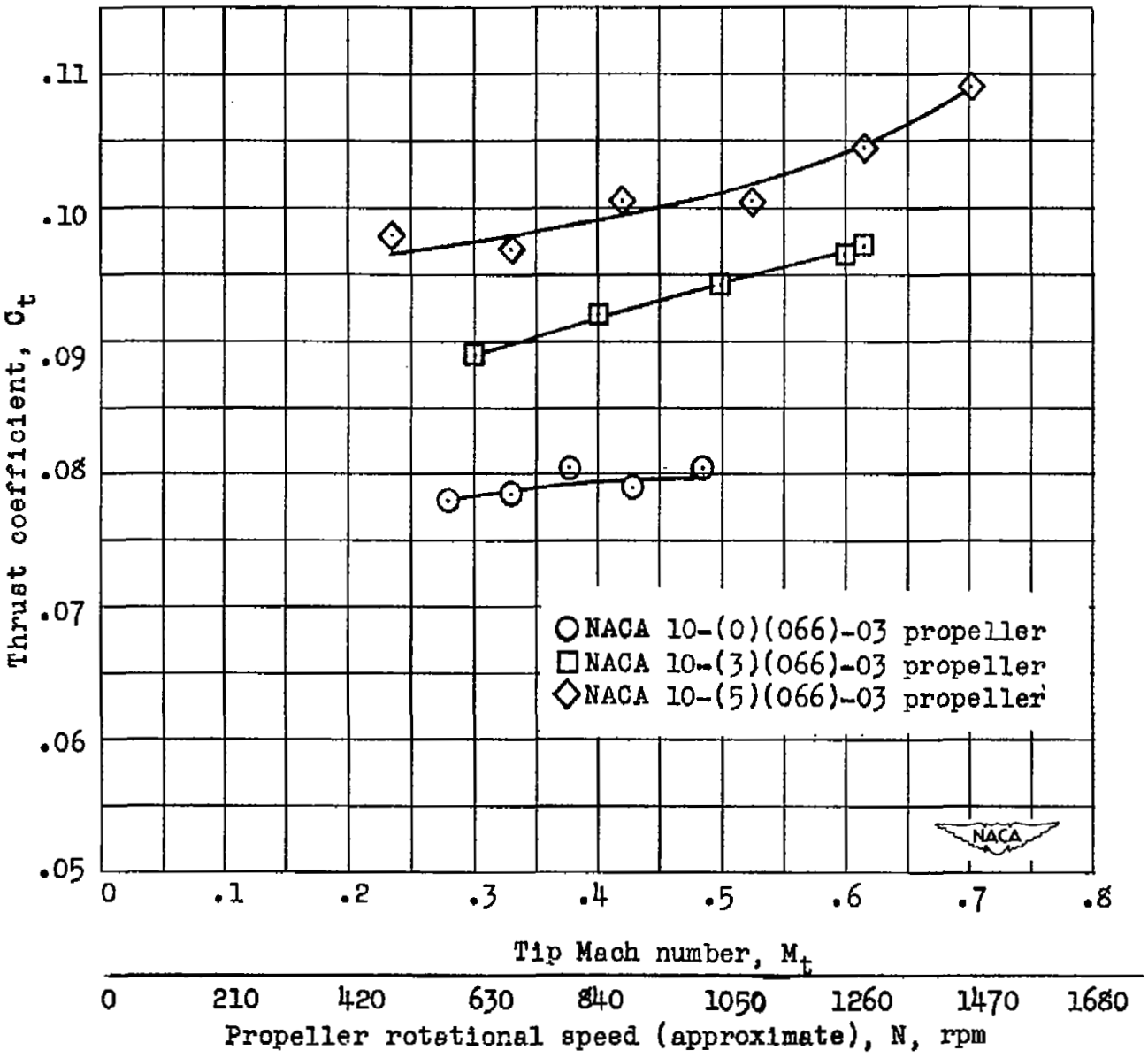

Figure 6.- Variation of thrust coefficient with tip Mach number (or approximate propeller rotational speed). $\beta_{0.75R} = 16^{\circ}$.

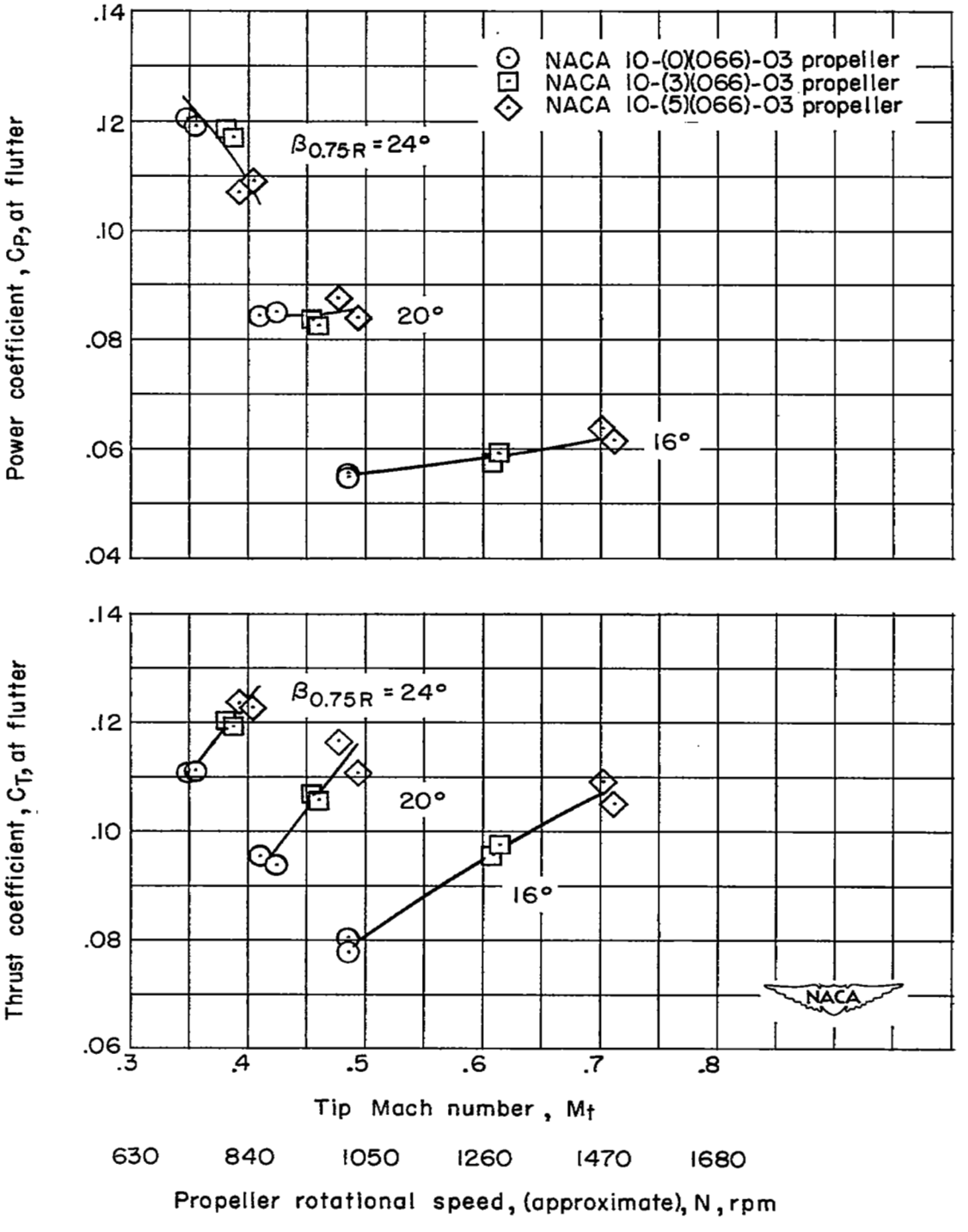

Figure 7.- Variation of thrust and power coefficient with tip Mach number (or approximate propeller rotational speed) at flutter.

[redacted]

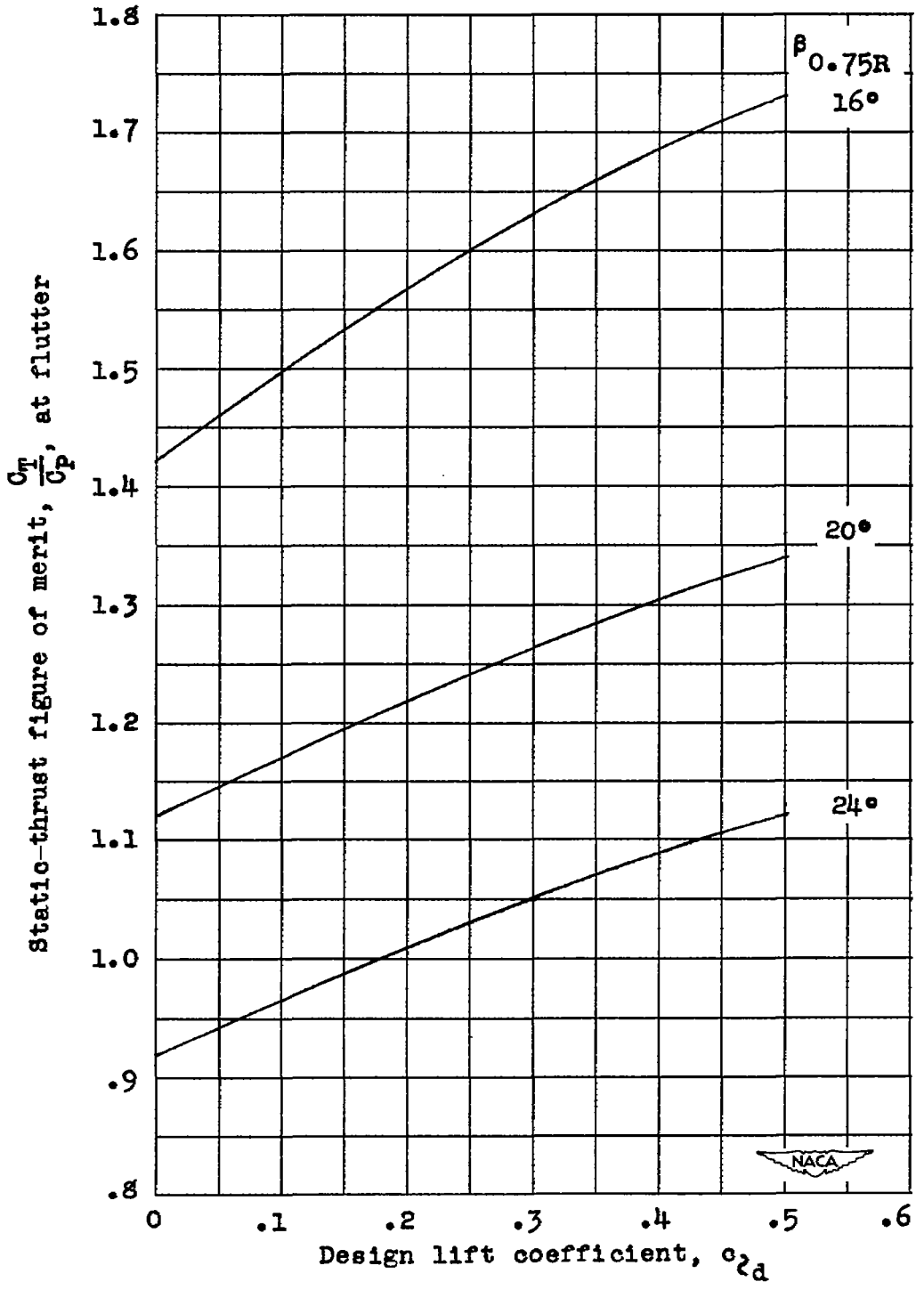

Figure 8.- Variation of static-thrust figure of merit with design lift coefficient at flutter.

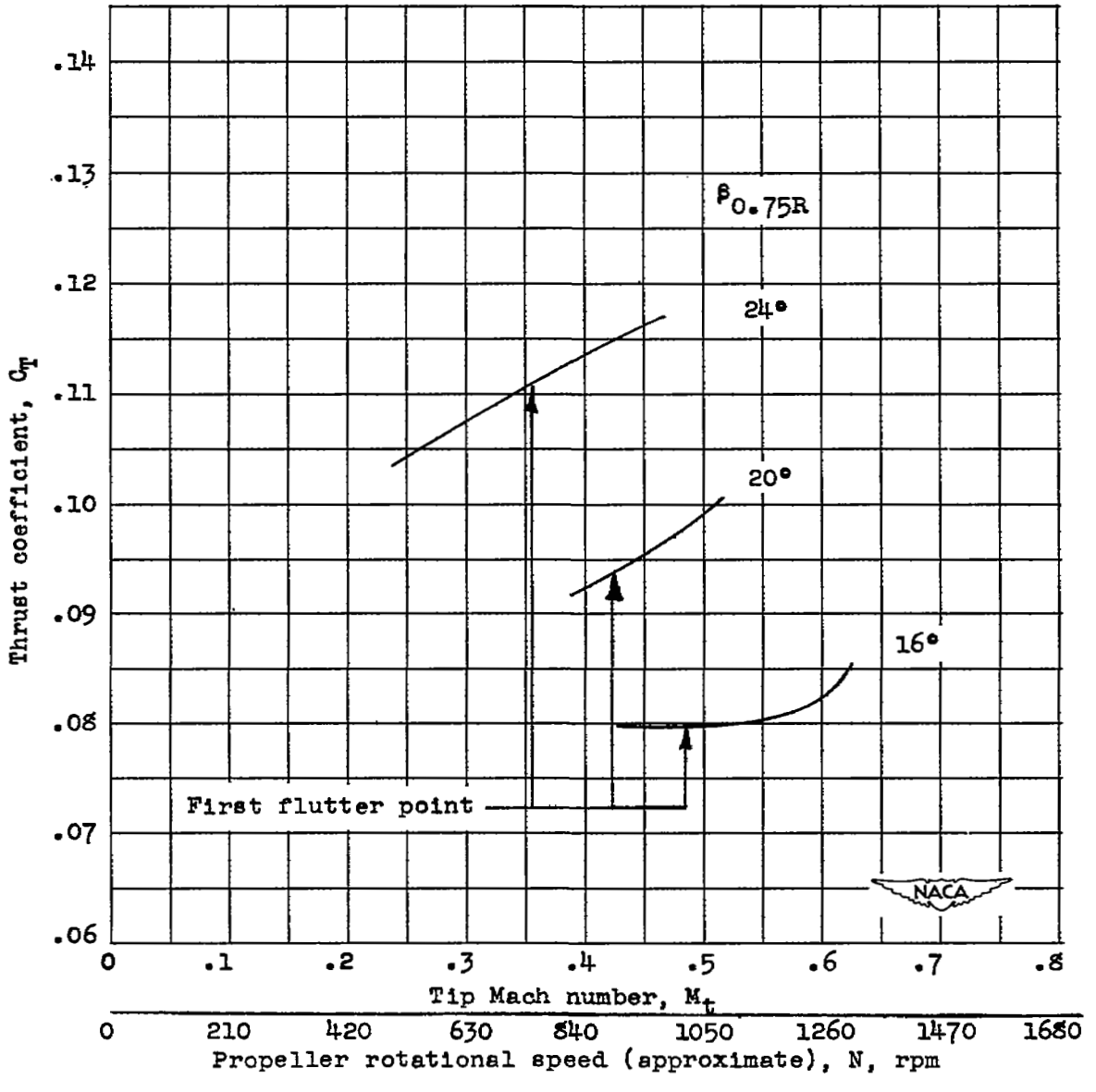

(a) Thrust coefficient, C_T.

Figure 9.- Variation of force characteristics with tip Mach number (or approximate propeller rotational speed) in the flutter region for the NACA 10-(0)(066)-03 propeller.

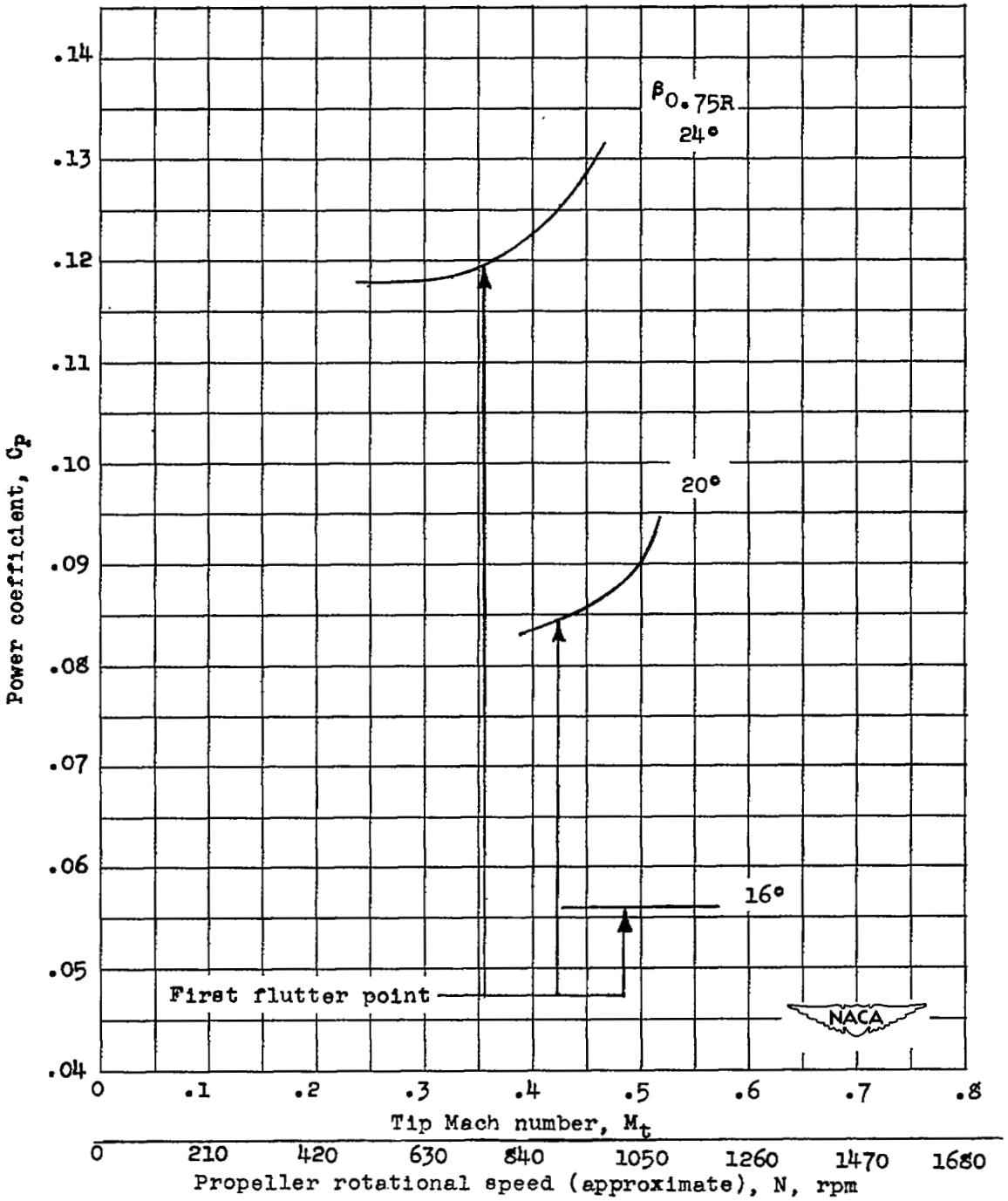

(b) Power coefficient, C_p.

Figure 9.- Continued.

[redacted]

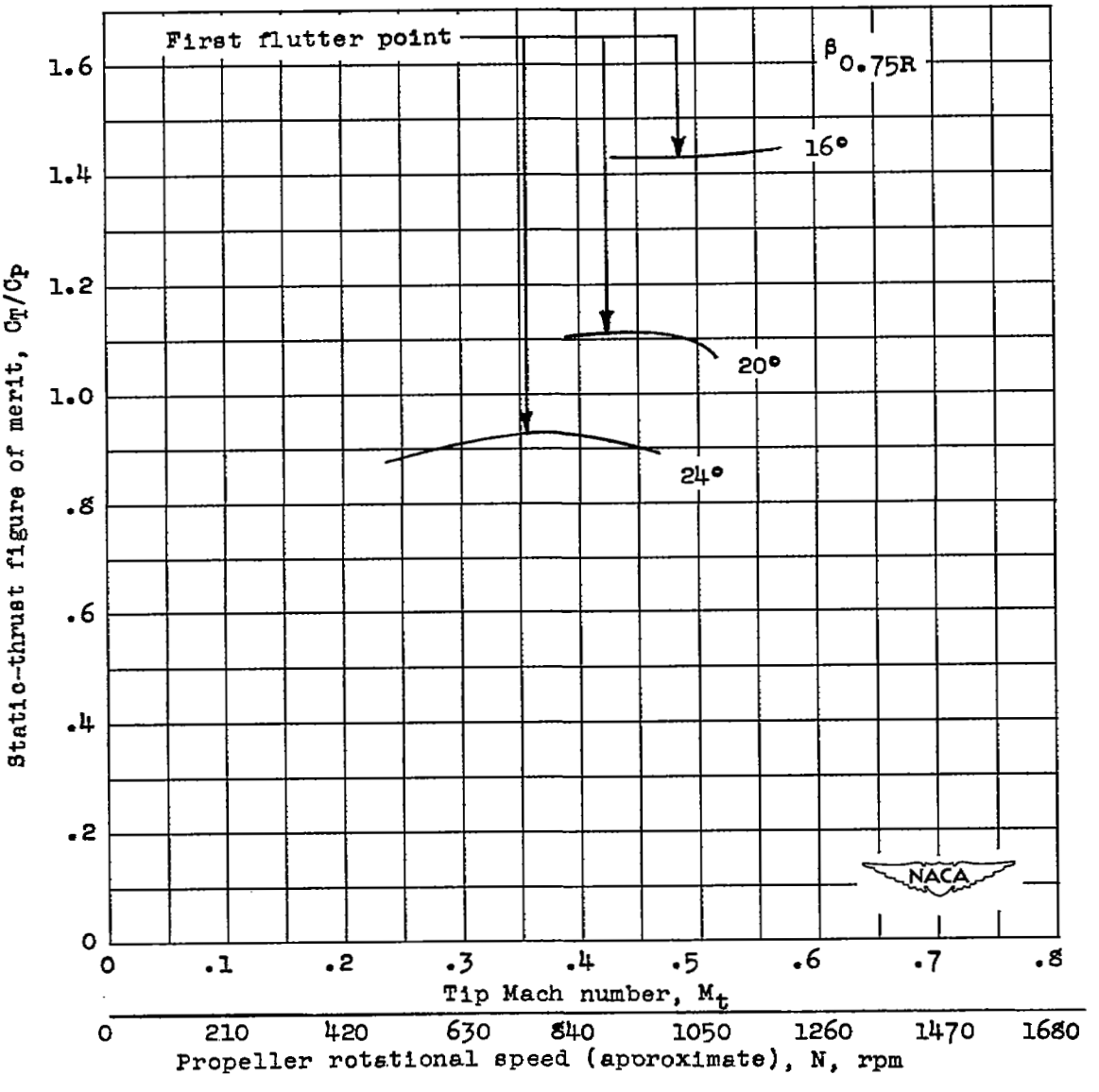

(c) Static-thrust figure of merit, C_T/C_p.

Figure 9.- Concluded.

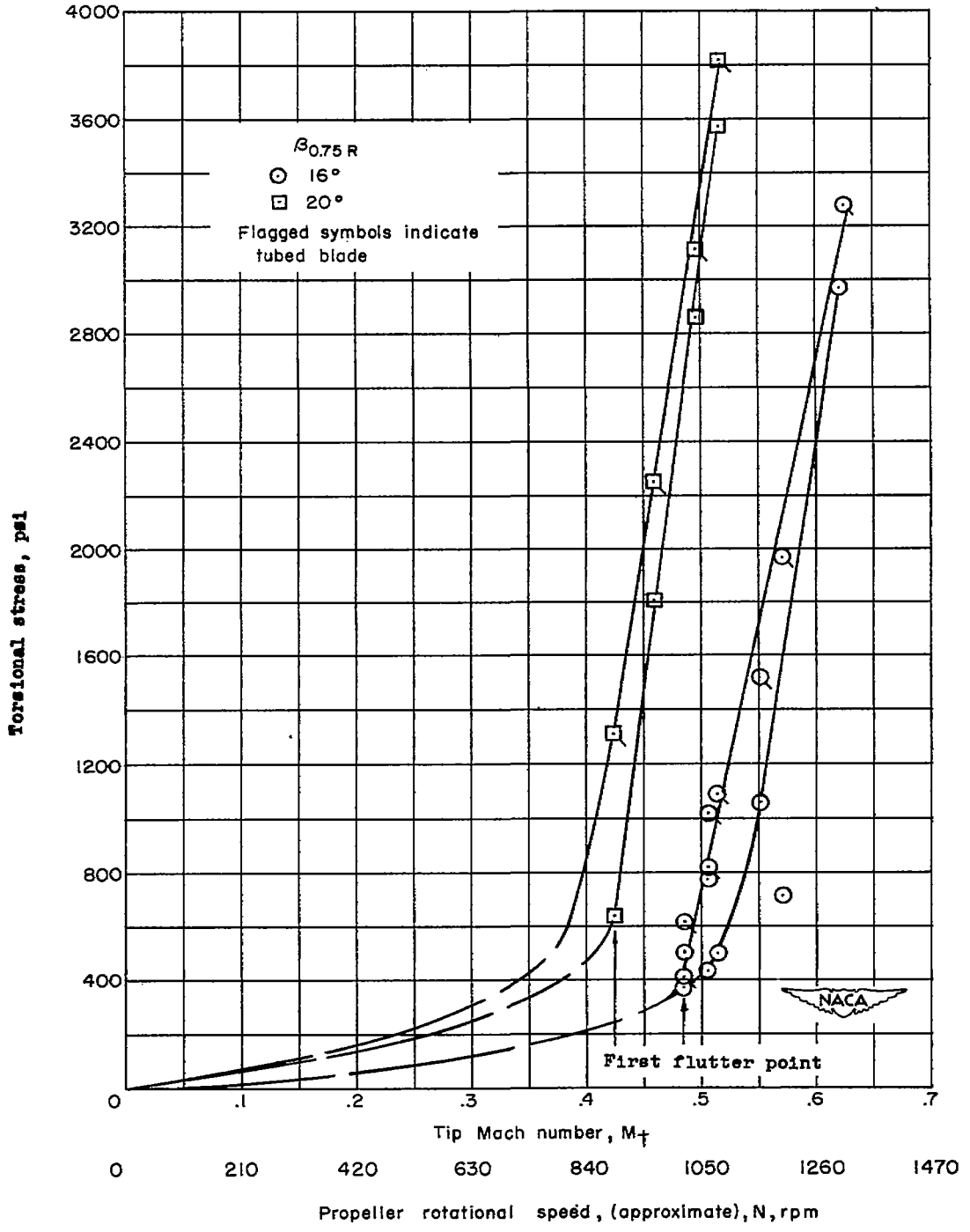

Figure 10.- Variation of torsional stress with an increase in tip Mach number (or approximate propeller rotational speed) for the NACA 10-(0)(066)-03 propeller.

[redacted]

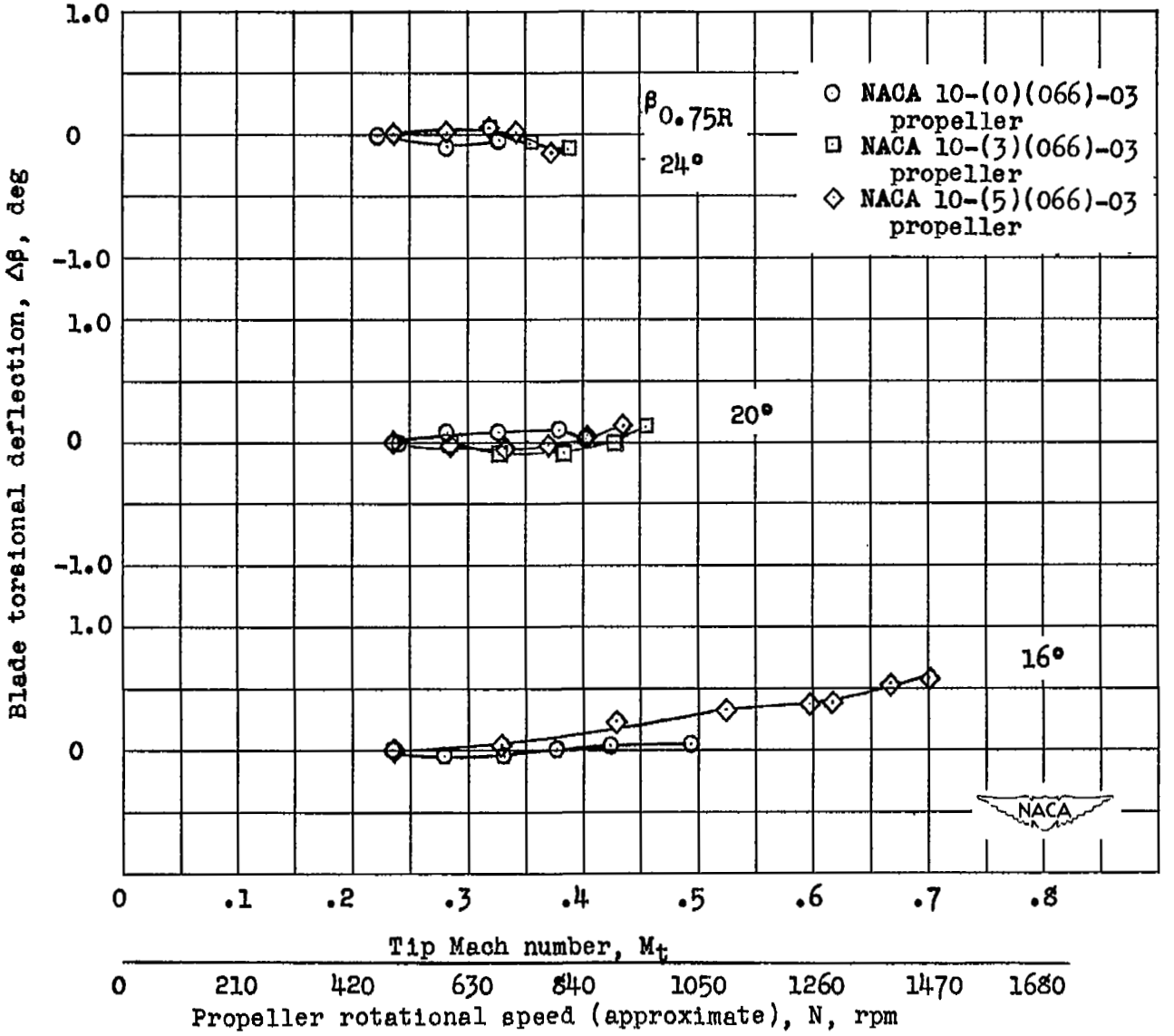

Figure 11.- Variation of blade torsional deflection with tip Mach number (or approximate propeller rotational speed) for the propellers tested.

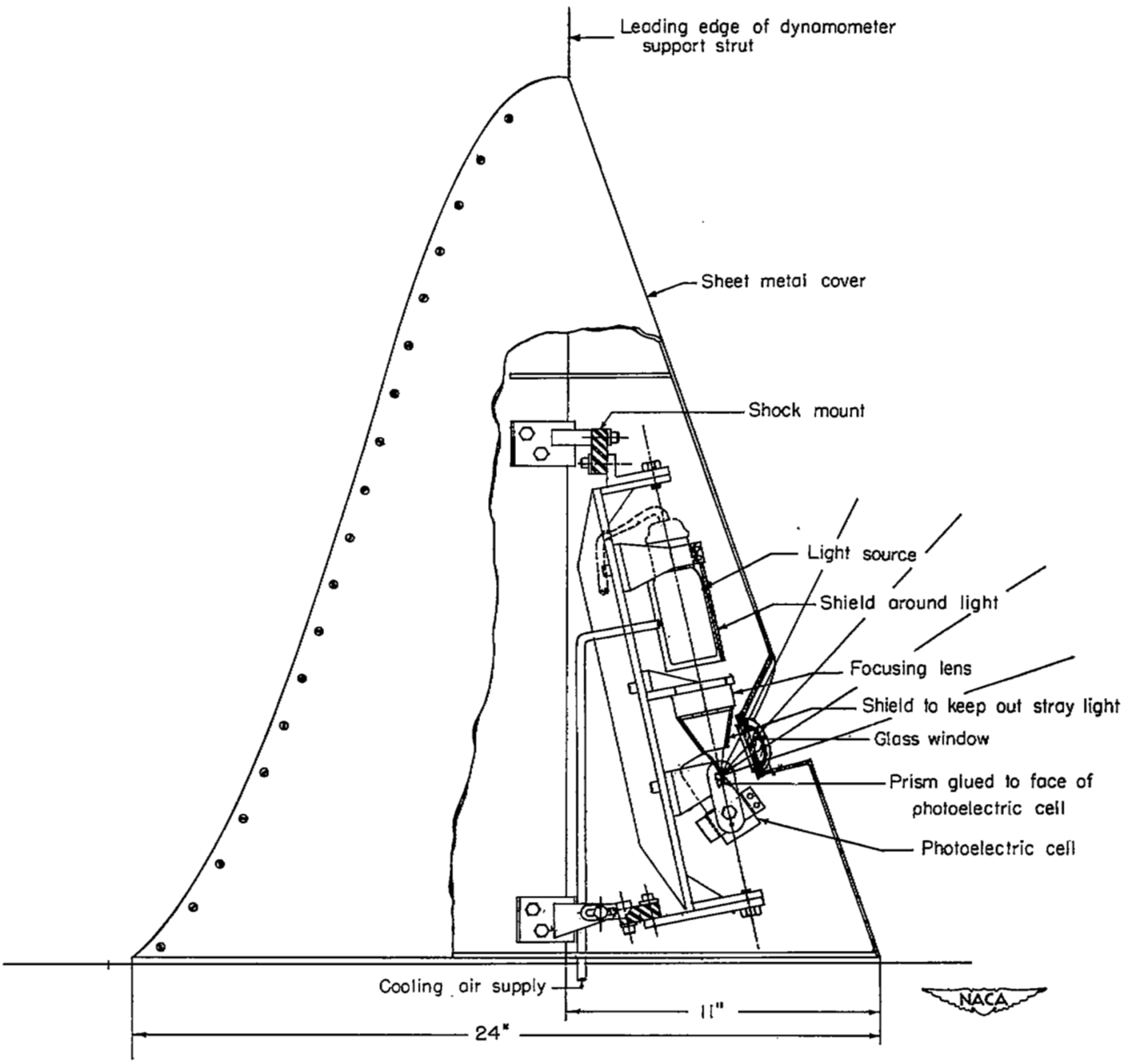

Figure 12.- Detail of deflectometer apparatus at base of dynamometer strut.

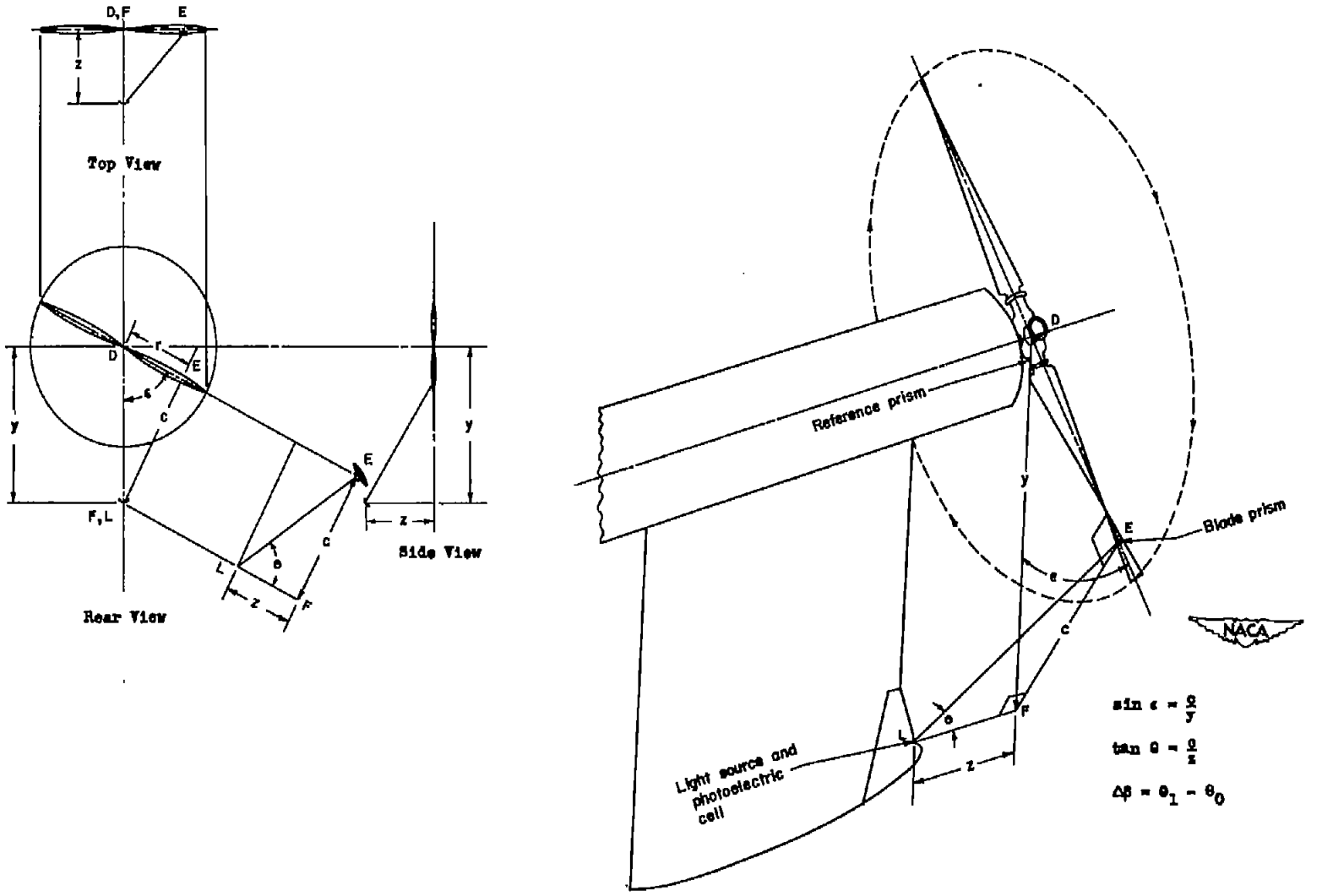

Figure 13.- Diagrams showing geometry used in measuring blade torsional deflections.